EFFECT OF PRESTRESSED FORCE AND SIZE OF REINFORCEMENT ON CORROSION CRACK WIDTH IN CONCRETE MEMBER

AGUS MARYOTO[1,*], TAKUMI SHIMOMURA[2]

[1]Department of Civil Engineering, Jenderal Soedirman University,
Jl. Mayjend Sungkono KM 5, Blater, Purbalingga, Central Java, Indonesia, 53371
[2]Department of Civil Engineering, Nagaoka University of Technology,
1603-1 Kamitomioka machi, Nagaoka, Niigata Prefecture, 940-2137, Japan
*Corresponding Author: agus_maryoto1971@yahoo.co.id

Abstract

One of the main factors which terminate service life of concrete structure in corrosive environment is corrosion attack. Rust expansion of corroded reinforcement in concrete causes corrosion crack. Crack width due to corrosion on the surface of concrete is influenced by some factors, i.e., prestressed force, size of reinforcement and thickness of concrete cover. Effect of prestressed force and size of reinforcement in corrosion crack width is investigated using numerical simulation based on elastic expansion model which is adopted to discover those influences. Three specimens of prestressed concrete beam and three specimens of reinforced concrete beam are utilized in the investigation. Experimental work is carried out to validate the numerical simulation results. It is found that prestressed force has insignificant influence on corrosion crack width. Meanwhile, size of reinforcement contributes greatly on crack width due to corrosion on the surface of concrete.

Keywords: Corrosion crack, Crack width, Prestressed force, Size of reinforcement.

1. Introduction

Millions of reinforced and prestressed concrete structures in the world located under corrosive environment suffer corrosion attack. As a consequence of concrete which is a porous material, sulphate, chloride and other aggressive agent infiltrate into concrete through the pores and capillaries. Reaction with oxygen they produce corrosive product on the surface of steel within concrete structures.

Abbreviations	
PC	Prestressed Concrete
PVC	Polyvinyl Chloride

Volume of corrosive product is greater than volume of the original steel. Expansion stress is then induced in concrete by corrosive product. As a result, corrosion crack will be generated in concrete, when the tensile stress induced by corrosive product exceeds the tensile strength of concrete [1 - 3].

Concrete around steel bar is induced by internal pressure due to expansion of corrosive product. It properties have an excessive impact on corrosion crack in concrete. Generally, volume of corrosive product is 2 – 8 times as much volume as virgin steel depending on content of corrosive product in it. The ratio of steel and the corrosive product in volume is known as the coefficient of corrosive product expansion. Some researchers employed the coefficient of corrosive product expansion around 3 [4]. The latest investigation of the coefficient of corrosive product expansion was conducted by Zhao et al. [5]. The coefficient has a range from 2.64 to 3.14. The specimens of corrosive product were taken from 8 different locations. Production of corrosive product in concrete member being electro-osmoses treated was 3.14. Physical characteristic like a gel is another important property of the corrosive product is stated by Andrade et al. [6].

Corrosive expansion is simulated in numerical analysis in terms of pressure or displacement at the surface of hole in concrete or thermal expansion of steel embedded in concrete. Some researchers have applied those models to verify their experimental results. Uniform internal pressure was adopted [7] to express radial expansion in concrete due to corrosion of steel bar. They modified boundary condition of support in order to express non uniform expansion of corroded steel. Internal displacement was applied as on Du et al. [8] to model corrosive expansion in reinforced concrete beam. They induced uniform and non-uniform internal displacement on the surface of inner hole of which diameter is same with the steel bar. The non-uniform internal displacement was set in regular shape to represent corrosive expansion.

Simulation of corrosive expansion of reinforcement considering properties of corrosive product was conducted by Molina et al. [9]. Two dimensional plane strain analysis was implemented. The value of 0.499 and 2000 MPa were adopted for Poisson`s ratio and modulus of elasticity of corrosive product respectively. Thermal load was applied in elastic material to express corrosive expansion of steel bar. Crack occurred on concrete cover due to expansion of elastic material.

This study attempts to investigate the effect of prestressed force and size of reinforcement in corrosion crack on the surface of concrete. Both numerical simulation and experimental work were conducted to treasure the effects on corrosion crack. An elastic expansion which was applied in the previous study [10] is adopted in this study.

2. Specimens

2.1. Effect of prestressed force

Table 1 shows the type of specimens which are investigated in this study. Figure 1 shows dimension and materials of the specimen [11]. A PVC pipe was utilized

as a sheath to protect the steel bar from corrosion attack. The specimens comprise 3 types which are PC-0, PC-2 and PC-4. The letter of 'PC' stands for prestressed concrete and the number following the letter 'PC', 0, 2, and 4 are to specify the prestressed force induced in the concrete. The number of specimen both in experimental work and numerical simulation is one for each type.

Table 1. Specimens for the effect of prestressed force [11].

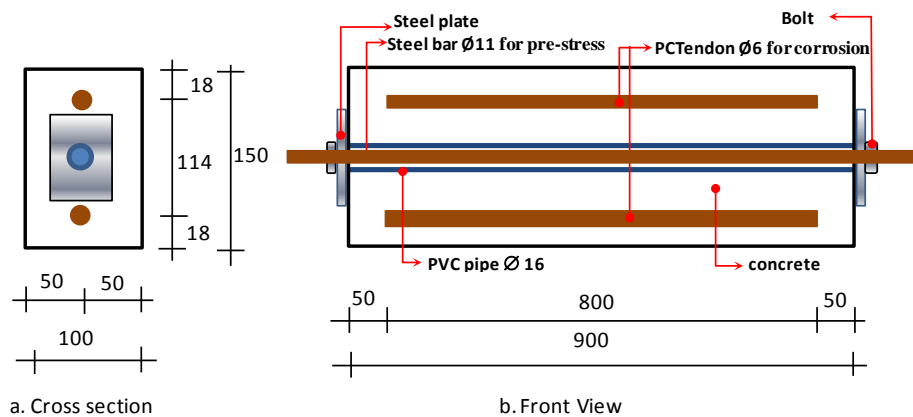| Specimen code	Prestressed force (N/mm^2)
PC-0	0
PC-2	2.33
PC-4	4.73

Fig. 1. Specimen for the effect of prestressed force [11].

Specifications of the materials are shown in Table 2. PC tendon and PC steel bar are tested based on Japan Industrial Standard [12]. Prior to cast fresh concrete into the form, the tendon ∅6 mm of each beam is weighed to obtain the initial weight. Specimens are cured being covered with wet mattress for 10 days. Compressive strength of concrete is tested by the cylindrical specimen whose dimension is 100 mm diameter and 200 mm height.

Table 2. Specification of materials.

Mechanical properties	Material		
	Concrete	Tendon ∅6 mm	Steel bar ∅11 mm
Young Modulus, E (MPa)	34070	20100	201000
Poisson (v)	0.2	0.3	0.3
Tensile Strength (MPa)	3.01	2018	1080
Compressive Strength (MPa)	32	-	-
Yield Strength (MPa)	-	1922	930

2.2. Effect of reinforcement size

Concrete beams dimension of $100 \times 100 \times 400$ mm^3 as shown in Fig. 2 is prepared. Figure 2(a) is a specimen with steel bar, Fig. 2(b) is a specimen with PC sheath without PC tendon inside and Fig. 2(c) is a specimen with a PC tendon. Reinforcements used in this experiment are steel bar D19 mm, PC sheath with $\varnothing$22 mm and 0.25 mm of thickness and PC tendon with $\varnothing$2.2 mm. Non-shrinkage grout MG-15M is used to fill inside of the PC sheath. Mixing ratio of water to powder is 18% by weight. Figure 3 shows the installation of reinforcements of steel bar and PC sheath in the casting mould. Proportion of concrete mixture is shown in Table 2.
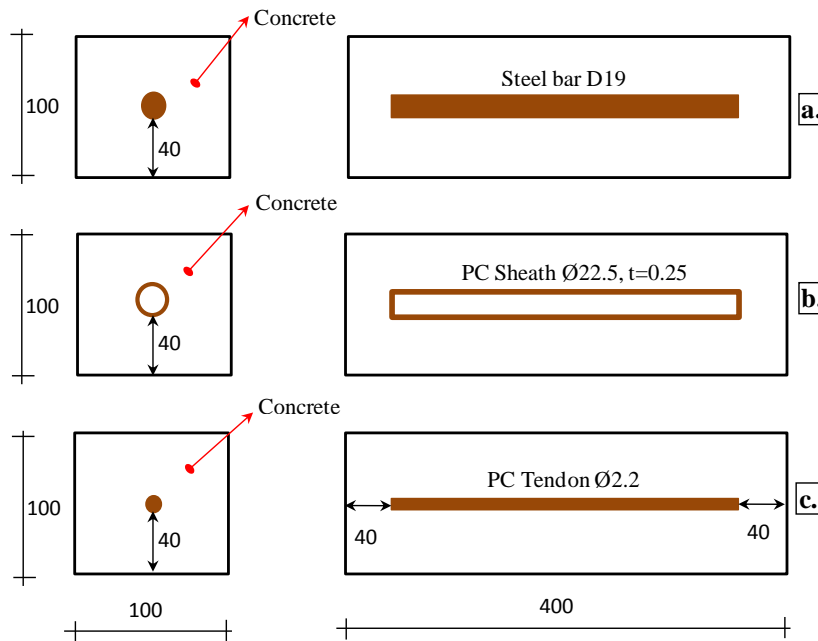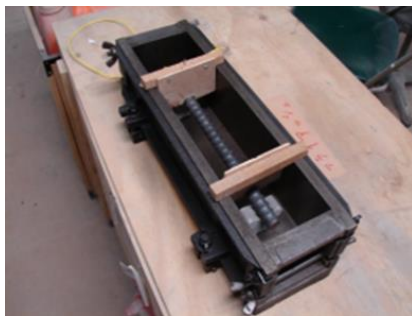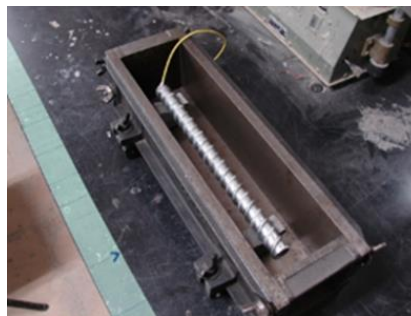
Fig. 2. Concrete specimens with steel bar, PC sheath and PC tendon.

a. Steel bar D19 mm. **b. PC sheath $\varnothing$22 mm.**

Fig. 3. Installation of reinforcement in moulding.

Table 3. Proportion of concrete mixture.

G_{max} (mm)	w/c (%)	s/a (%)	Unit weight (kg/m^3)				Additive (ltr/m^3)
			water	cement	sand	gravel	
25	39.5	35.5	154	390	622	1189	3.9

where G_{max} is maximum size of aggregate, *w/c* is water/cement ratio in weight, s/a is sand/total aggregate volume ratio, cement is early strength type, additive is water reducing agent.

3. Numerical Simulation

3.1. Constitutive model of concrete

Tensile stress and strain relationship in Fig. 4 is adopted for concrete [11]. Before cracking, relationship between stress and strain is linear. When tensile stress reaches the tensile strength of concrete, crack is developed in concrete. Tensile stress decreases after cracking generated. The strain was proposed by Reinhardt [13], where softening curve is expressed by non-linear function as in Eq. (1). Constitutive model for concrete in compression is shown in Fig. 5. The relationship between stress and strain for short-term uniaxial compression is defined by Eq. (2) based on CEB [14].

$$f_t = \frac{E}{1-x^{c_1}} \quad \text{where} \quad x = \frac{\varepsilon^{cr}}{\varepsilon_{ult}}, \quad c_1 = 0.31 \tag{1}$$

where, ε^{cr} is the crack strain ε_{ult} is the ultimate crack strain, and *h* is crack bandwidth. Uniaxial tensile strength (f_t), modulus of elasticity (E) and fracture energy (G_f) of concrete are estimated from compressive strength ($f'c$) and maximum aggregate size as stated in [14].

$$\frac{\sigma_c}{f_{cm}} = -\left(\frac{k.\eta - \eta^2}{1+(k-2).\eta}\right) \text{ for } |\varepsilon_c| < |\varepsilon_{c,lim}| \tag{2}$$

where $\eta = \frac{\varepsilon_c}{\varepsilon_{c1}}$ and $k = \frac{E_{ci}}{E_{c1}}\varepsilon_c$

and ε_{c1} is the strain at maximum compressive stress, E_{c1} is the secant modulus from the origin to the peak compressive stress and *k* is the plasticity number.
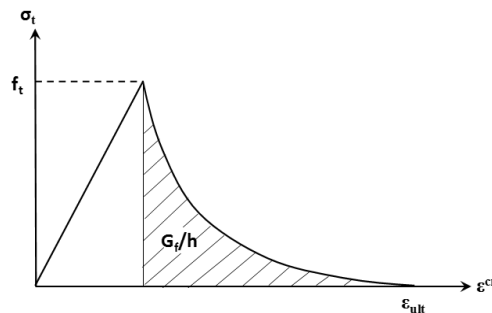
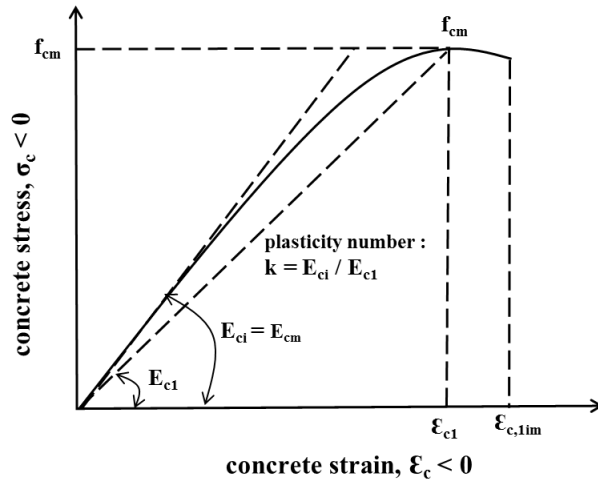

Fig. 4. Constitutive model for concrete in tension.

Fig. 5. Constitutive Model for concrete in compression.

3.2. Modelling of corrosive expansion of steel

It is assumed that the corrosive product uniformly expands as shown in Fig. 6 and Eq. (3) under unrestraint condition.

$$\frac{\pi(r_0 + dr)^2 - \pi.r_0^2}{\gamma - 1} = \pi.r_0^2 - \pi(r_0 - \Delta r)^2 \qquad (3)$$

where, dr is the radius increment of steel due to corrosive expansion under unrestraint condition (mm), Δr is the radius loss of steel (mm), r_0 is the original radius of steel (mm) and γ is the expansion coefficient of corrosive product. The ratio between volume of corrosive product and volume of steel consumed (γ) is determined based on the experiment of Zhao et al. [5], which is equal to 3.14. Corroded steel is converted into mass loss by following equation.

$$W_{loss} = \frac{[\pi.r_0^2 - \pi(r_0 - \Delta r)^2].\rho_s}{2\pi.r_0} = \frac{[2r_0.\Delta r - \Delta r^2].\rho_s}{2r_0} \qquad (4)$$

where, W_{loss} is mass loss in gr/mm^2 and ρ_s is mass density of PC tendon (0.00785 gr/mm^3). Both steel and corrosive products are treated as elastic material.
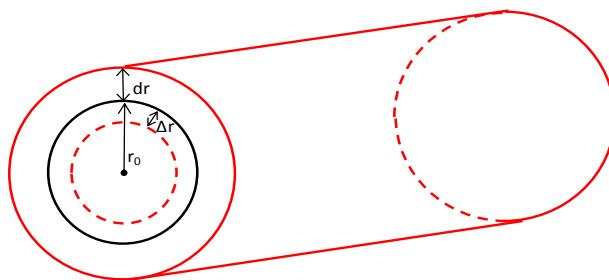

Fig. 6. Corrosive expansion of steel.

The numerical analysis is executed by the finite element code Diana-version 9.4.4 [15]. The specimen is modeled using eight-node isoparametric solid brick element. The finite element mesh is shown in Fig. 7 [11]. External compressive loads are applied to the specimen in the longitudinal direction as shown in Fig. 8 to simulate prestressed force [16] by the PC tendon. The reduction of the prestressed due to corrosion is not considered [17]. Therefore, effect of the bond between concrete and PC tendon is modeled as perfect bond. It is because the element mesh of PC tendon and concrete is connected continuously.
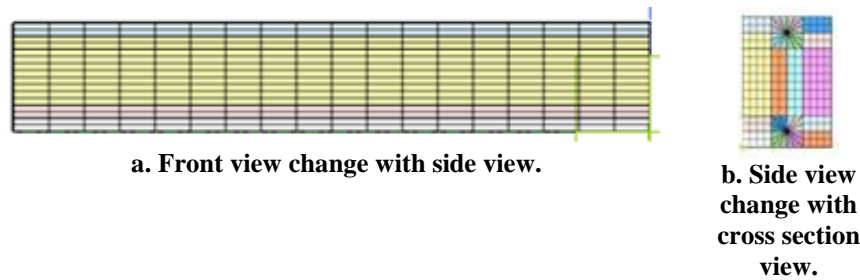

a. Front view change with side view.

b. Side view change with cross section view.
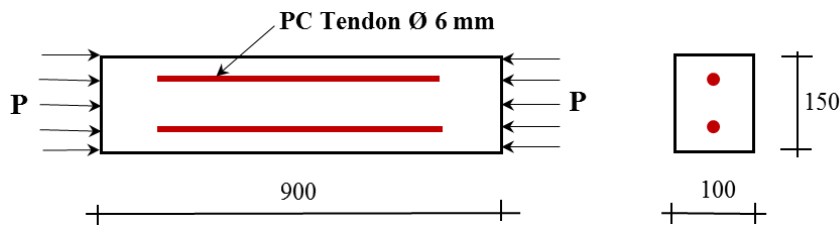
Fig. 7. The finite element mesh of specimen.

Fig. 8. External compressive loads.

4. Experimental Work

4.1. Electrolytic corrosion test

Specimens of concrete beam are covered with wet mattress for 28 days after being cast. Compressive strength of concrete is tested by the cylindrical specimen whose dimension is 100 mm diameter and 200 mm height.

Electrolytic corrosion test is conducted to produce rust in short time. Specimens are immersed in water containing 3% sodium chloride (3% NaCl) solution as an electrolyte. Figure 9 shows a scheme of the electrolytic corrosion test. Direct electric current is applied to promote corrosion process. After the corrosion test is completed, the specimens is broken and the corroded steel bar, PC sheath and PC tendon are taken out. Rust is removed using a wire brush and then the steel bar; PC sheath and PC tendon are immersed in the 10% ammonium citrate solution for one day. Thereafter, mass loss of the steel bar, PC sheath and PC tendon is measured by subtracting their initial weight from their final weight [11].
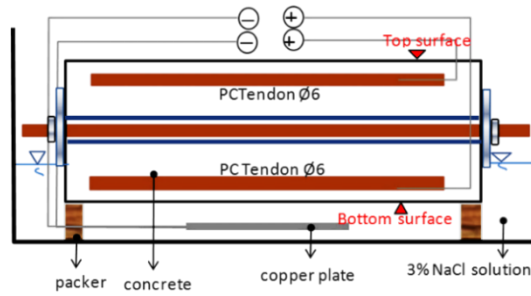
a. Effect of prestressed force [11].
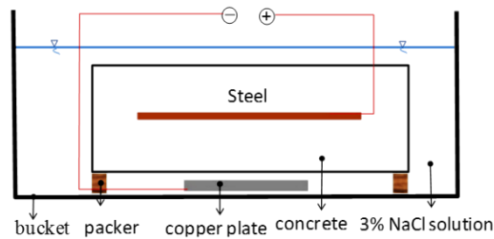
b. Effect of size of reinforcement.

Fig. 9. Scheme of electrolytic corrosion test.

4.2. Measurement of crack width and mass loss of steel

Only cracks on the bottom surface, Fig. 9(a) are considered. The occurrence of cracks is monitored every day. The occurrence of the first crack was judged when the crack width reached 0.01 mm. Thereafter, crack width is measured using a manual scale at 3 points of the beam, which are in the center, 100 mm to left and right from the center of the beam. Average crack width of those 3 points is discussed.

Electric current induced in the corrosion test is recorded in the data logger every 30 minutes. Accumulative current ($\Sigma I.T$) is calculated at the end of corrosion test. The amount of corrosion of the PC tendon can be predicted using equation below based on the Faraday's law.

$$W = \alpha . \Sigma I.T \tag{5}$$

where W is the amount of corrosion of the PC tendon (gr), α is a coefficient of electrolytic corrosion (gr/A.hr), I is electric current (A) and T is time (hr.). The coefficient of electrolytic corrosion is 1.0744 gr/A.hr. It is calculated according to $\alpha = M / (z.F)$, where M is the atomic mass of the metal (Fe = 56 gr), z is the ionic valence of the metal (Fe = 2) and F is Faradays constant (96,485 A.s). Thereafter, mass loss of the tendon is calculated by subtracting its initial weight

from the weight after being corroded. Mass loss of the tendon during the corrosion is estimated from the accumulative current at the time.

5. Result and Discussion

5.1. Effect of prestressed force

Table 4 shows the amount of corrosion of PC tendon when the first crack appears on the surface of concrete in the experiment work and in the analysis. It is found that the occurrence of crack in the specimen with greater prestressed is a little faster than in the specimen with lower prestressed. This phenomenon can be explained by Poisson's effect. Concrete beam are compressed in the longitudinal direction due to prestressed force and simultaneously tensioned in the lateral directions.

The pattern of the first crack can be seen in the Fig. 10 [11]. Both in the experiment work and in the numerical simulation, the crack appears on the centre of the beam. In the experiment, the first crack on surface can be seen with eyes, but its width is as small as 0.05 mm which is the minimum of the scale used. Green and red colours in the numerical simulation crack pattern indicate that crack width whose range is between 0.0026 mm - 0.0173 mm and 0.0173 mm – 0.0321 mm respectively.

Table 4. Amount of corrosion at the first crack on the surface.

Type of beam	Analytical (10^{-4} gr/mm^2)	Experimental (10^{-4} gr/mm^2)
PC-0	0.195	4.432
PC-2	0.176	3.909
PC-4	0.138	3.886

a. Experimental.
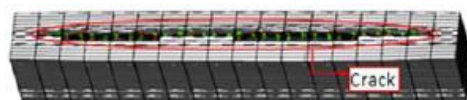
b. Numerical.

Fig. 10. Appearance of first crack on the surface of concrete [11].

Figure 11 shows the relationship between the corrosion of PC tendon and the crack width. In all of the numerical simulation results, the crack widths are almost proportional to the corrosion of PC tendon after the cracks are developed on surface of concrete. The compressive stress contributes to the initiation and opening of the crack [8].
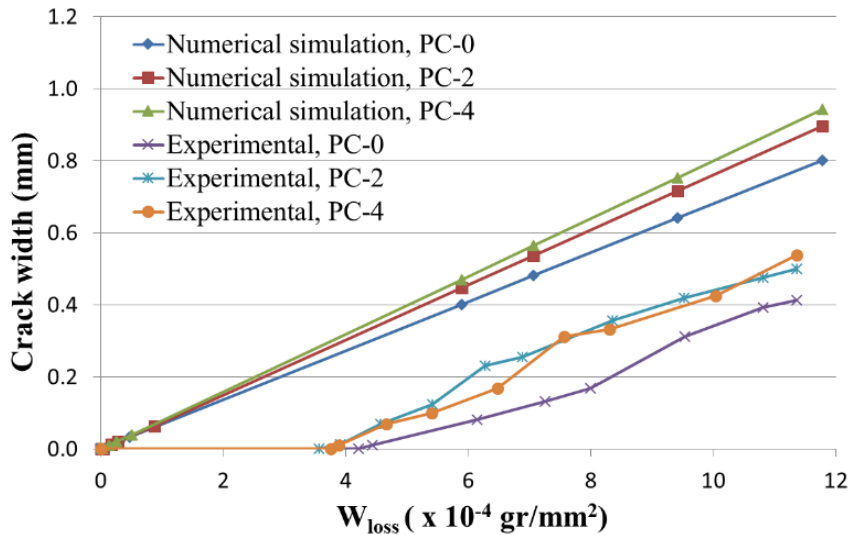
Fig. 11. Corrosion of PC tendon in concrete beam.

However, the effect of prestressed force on the corrosion crack is not remarkable. The comparison of the results between numerical simulation and experimental shows that experimental crack width is smaller than numerical simulation one. For example, corrosion crack width is observed when the corrosion level reaches 9 gr/mm^2. At this level of corrosion, the crack widths of the analytical result are 0.61 mm, 0.65 mm and 0.68 mm for PC-0, PC-2 and PC-4 respectively, while in the experiment, around 0.19 mm, 0.38 mm and 0.36 mm for PC-0, PC-2 and PC-4, respectively. This may be caused by the assumption in the calculation of the pressure by corrosive product is elastic while in reality, some corrosive product penetrates into concrete pore and cracks. Consequently, the actual pressure may not be proportional to the amount of corrosion on PC tendon. It can be also observed that the effect of compressive stress on the formation of corrosion crack width is very small. The cracks start on the surface of concrete in the experimental work when the level of corrosion reaches around 4×10^{-4} gr/mm^2. It can be understood because parts of corrosive product infiltrate into the pores and inner crack before the cracks propagate until the surface of concrete. The elastic model of corrosive product will be enhanced in the next work using the apparent amount of corrosive product to cover penetration of corrosive product into interface steel and concrete, pores and cracks [11].

5.2. Effect of size of reinforcement

Table 5 shows corroded mass of steel (W_{loss}) when the first crack occurs on the surface of concrete by numerical simulation. The earliest occurrence of crack on the surface of concrete was on the specimen with PC sheath, then followed by the specimen with steel bar and the last was the specimen with PC tendon. The results show that increasing of diameter of steel reinforcement corroded mass of steel necessary to generate crack decreases.

Table 5. Corroded mass of steel.

	Specimen		
	PC Tendon Ø2.2 mm	**Steel Bar D19 mm**	**PC Sheath Ø22 mm**
W_{loss} (10^{-4} gr/mm²)	1.0	0.7	0.3

Relationship between corroded mass of steel (W_{loss}) and crack width is shown in Fig. 12. It shows that, at the same corrosion level, the widest crack is developed in the specimen of PC sheath, then followed by of steel bar and PC tendon is the last. The increasing of crack width on the surface shows the same tendency with the onset of the first crack.

The result shows that, even though the diameter of PC tendon embedded in concrete is very small, it is enough to produce crack on the surface of concrete. This tendency can be also regarded in specimen of PC sheath. Though, the thickness of PC sheath is very thin, corrosion crack appears on the surface of concrete.

Another important point is that there is great difference between the experimental and analytical results. Calculated corrosion crack width is greater than experimental one. It is because linear expansion of elastic material was assumed in the numerical simulation. Penetration of corrosive product into the interface between reinforcement and concrete pores and inner micro cracks, which may reduce expansive pressure, does not simulated by this model.
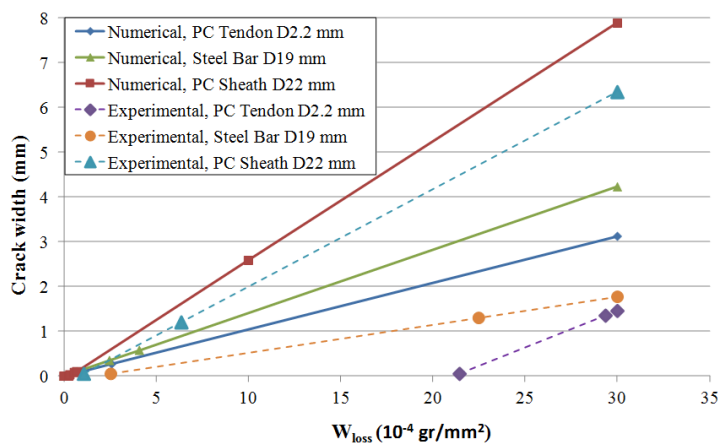

Fig. 12. Crack width as function of W_{loss}.

Figure 13 shows experimentally observed crack pattern of the specimens. Corrosion crack appears on the center of the specimen along the reinforcement. The crack appears when percentage of corroded steel is 68%, 7% and 34% in weight for the specimen with PC tendon, steel bar and PC sheath respectively. The tendency of influence of size of corroded steel in the experimental results is similar with that in the analytical results.
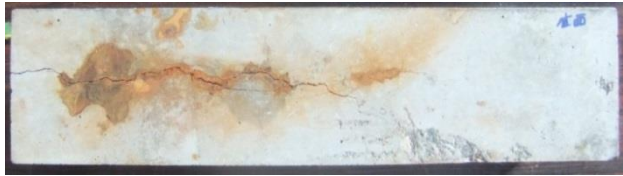
a. Specimen with PC sheath.

b. Specimen with steel bar.

c. Specimen with PC tendon.

Fig. 13. Crack pattern of the experimental specimens.

6. Conclusions

According to the results of the numerical simulation and experimental investigation on corrosion crack in concrete members, following conclusions are obtained as below.

- Compressive stress in the longitudinal direction accelerates development and opening of corrosion crack, but the effect is very small.
- Compressive stress in concrete by prestressed force in prestressed concrete member does not have influence significantly on development and opening of corrosion crack in actual structure.
- The size of reinforcement embedded in concrete affects corrosion crack on the surface of concrete.
- The small diameter of steel reinforcement or the thin of PC sheath generate crack on surface of concrete.
- The next numerical simulation using the elastic expansion model is promoting to improve the penetration of corrosive product into the pore and cracks of concrete and also the interfacial space between reinforcement and concrete.

References

1. Maryoto, A.; Buntara, S.G.; and Aylie, H. (2017). Reduction of chloride ion ingress into reinforced concrete using a hydrophobic additive material. *Jurnal Teknologi,* 79(2), 65-72.

2. Maryoto, A. (2017). Resistance of concrete with calcium stearate due to chloride attack tested by accelerated corrosion. *Procedia Engineering* (under published process).

3. Maryoto, A. (2015). Improving microstructure of concrete using $Ca(C_{18}H_{35}O_2)_2$. *Procedia Engineering*, 125, 631-637.

4. Lu, C.; Jin, W.; and Liu, R. (2011). Reinforcement corrosion-induced cover cracking and its time prediction for reinforced concrete structures. *Journal of Corrosion Science*, 53(4), 1337-1347.

5. Zhao, Y.; Ren, H.; Dai, H.; and Jin, W. (2011). Composition and expansion coefficient of rust based on X-ray diffraction and thermal analysis. *Journal of Corrosion Science*, 53(5), 1646-1658.

6. Andrade, C.; Tavares, F.; Toro, L.; and Fullea, J. (2011). *Observation on the morphology of oxide formation due to reinforcement corrosion*. A chapter in the book: Modelling of Corroding Concrete Structures, Volume 5 of the Series RILEM Bookseries, 179-193.

7. Zhao, Y.; Karimi, A.R.; Wong, H.S; Hu, B.; Buenfield, N.R.; and Jin, W. (2011). Comparison of uniform and non-uniform corrosion induced damage in reinforced concrete based on a Gaussian description of the corrosion layer. *Journal of Corrosion Science*, 53(9), 2803-2814.

8. Du, Y.G.; Chan, A.H.C.; and Clark, L.A. (2006). Finite element analysis of the effect of radial expansion of corroded reinforcement. *Computer and Structures*, 84(13-14), 917-929.

9. Molina, F.J.; Alonso, C.; and Andrade, C. (1993). Cover cracking as a function of rebar corrosion: part 2 – numerical model. *Material & Structures,* 26(9), 532-548.

10. Maryoto, A.; Kitazono, Y.; and Shimomura, T. (2011). Numerical simulation of corrosion crack in reinforced concrete (RC) and pre-stressed concrete (PC) member. JSCE - Kanto Branch, Niigata Conference, Japan, 378-381.

11. Maryoto, A.; and Shimomura, T., (2015). Prediction of crack width due to corrosion of PC tendon in prestressed concrete structure. *Civil Engineering Dimension*, 17(2), Christian Petra University, Indonesia, 67-75.

12. Anonym, (2008). *Steel bars for prestressed concrete*. Japan Industrial Standard G 3109, Japan.

13. Reinhardt, H.W. (1984). *Fracture mechanics of an elastic softening material like concrete*. Heron 29, 2.

14. Anonym, (1990). *Committee Euro-International du Beton – Federation Internationale de la Precontrinte*. CEB-FIP Model Code, Thomas Telford Ltd, London.

15. Diana, (2010). *User's manual*. Release 9.4.4, TNO DIANA, BV, Delft, The Netherlands.

16. Haryanto, Y.; Buntara, S.G.; and Maryoto, A. (2017). Wire rope flexural bonded strengthening system on RC-beams: a finite element simulation. *International Journal of Technology*, 8(1), 132-142.

17. Maryoto, A.; Hermanto, N.I.S.; Haryanto, Y.; Waluyo, S.; and Anisa, N.A. (2015). Influence of prestressed force in the waste tire reinforced concrete. *Procedia Engineering*, 125, 638-643.